*Progress In Electromagnetics Research B, Vol. 77, 57–69, 2017*

# Loop Antennas with Uniform Current in Close Proximity to the Earth: Canonical Solution to the Surface-to-Surface Propagation Problem

**Mauro Parise[1, *], Marco Muzi[1, 2], and Giulio Antonini[3]**

**Abstract**—In a recent study, the classical problem of a large circular loop antenna carrying uniform current and situated at the Earth's surface has been revisited, with the scope to derive a totally analytical explicit expression for the radial distribution of the generated magnetic field. Yet, the solution arising from the study exhibits two major drawbacks. First, it describes the vertical magnetic field component only. Second, it is a valid subject to the quasi-static field assumption, which limits its applicability to the low-frequency range. The purpose of the present work is to provide the exact canonical solution to the problem, describing all the generated electromagnetic field components and valid in both the quasi-static and non-quasi-static frequency regions. These two features constitute an improvement with respect to the preceding solution. The canonical solution, which is obtained by reducing the field integrals to combinations of known Sommerfeld integrals, is seen to be also advantageous over the previous numerical and analytical-numerical approaches, since its usage takes negligible computation time. Numerical simulations are performed to show the accuracy of the obtained field expressions and to investigate the behavior of the above surface ground- and lateral-wave contributions to the fields in a wide frequency range. It is shown that in the near-zone the two waves do not predominate over each other, while the effect of the lateral wave becomes negligible only when the source-receiver distance is far greater than the skin depth in the Earth.

## 1. INTRODUCTION

In the last decades, large circular loops of wire have found extensive application in a number of fields of scientific and technological interest, including radio communication, radio remote sensing, geophysical prospecting, amplitude modulation broadcasting, radio direction finding, diathermy. Correspondingly, a large body of literature has been dedicated to the study of the radiation from these sources [1–24], and many approaches have been proposed for accurately evaluating the integral representations describing the generated EM field components. A portion of the published papers deals with sources carrying uniform currents, either lying in free-space or in presence of stratified material media [1–4, 7, 9, 10, 12]. Even if contributions in that direction are naturally tailored only to electrically small loops, their validity may be extended to loops of any size relative to the wavelength, provided that the feed system can ensure a nearly uniform current distribution along the wire. Different techniques make it possible to obtain this result, and most of them have been known since 1940s [1, 24]. The simplest method consists of dividing the periphery of the antenna into segments that are short in comparison with the wavelength, and driving such segments in parallel by means of radial transmission lines [1]. In spite of the simplicity of the antenna geometry, exact analytical explicit expressions for the radiated fields are, to date, available

*Received 20 April 2017, Accepted 10 July 2017, Scheduled 24 July 2017*
* Corresponding author: Mauro Parise (m.parise@unicampus.it).
[1] Unit of Electrical Engineering, University Campus Bio-Medico of Rome, Italy. [2] Department of Information Engineering, Electronics and Telecommunications, "La Sapienza" University of Rome, Italy. [3] Department of Industrial Engineering, Computer Science and Economics, University of L'Aquila, Italy.

only for the free-space case [1–3, 9]. When, instead, the circular loop is located horizontally above or on ground structures, integration of the field integrals becomes difficult and impractical. Explicit solutions can still be derived, but are either valid subject to restrictive assumptions (on the operating frequency or the observation points, for instance), or are accurate everywhere but not completely analytical, and, as a consequence, time consuming. Examples of the former are the small-loop approximations for the fields [25, 26] and the quasi-static approximation for the vertical magnetic field [16], valid only in the near zone of the antenna. On the other hand, excellent illustrations of the latter are the series-form representations arising from applying digital filter technique [4, 18, 22] and Newton's method [10, 12], which, before being used, require the a-priori computation of a large set of numerical coefficients.

The present work focuses on the derivation of the complete canonical solution to the problem of a large horizontal circular loop antenna carrying uniform current and lying on a conducting semi-infinite half-space. The surface-to-surface propagation case is considered, and the solution is derived through a totally analytical procedure, which permits to rewrite the field integrals in a form that involves only previously evaluated Sommerfeld Integrals. As a result, both the electric and vertical magnetic fields are given as sums of two terms, each one consisting of a series of spherical Hankel functions of the second kind. The two terms describe the contributions of the above-surface ground wave and lateral wave generated by the loop. Instead, the radial magnetic field component is expressed in terms of modified Bessel functions. It is easily understood how useful physical insight can be gained by investigating the expressions for the field components, and this, combined with the possibility to rapidly perform any parametric analysis, makes the derived solution advantageous with respect to any numerical simulation tools employed to solve electromagnetic boundary value problems. Moreover, the obtained solution permits fast and accurate calculation of the radiated fields regardless of the operating frequency and the position of the field point, and without requiring the a-priori computation of a set numerical coefficients. This makes the solution advantageous over any previously published approach to solve the same problem [4, 10, 12, 18, 22]. Finally, a glance at the far-field asymptotics of the solution reveals that ground and lateral waves have the characteristics of cylindrical waves travelling in the positive radial direction. Their analytical expressions are formally similar to those describing the fields of the loop in free-space, except for the functional dependence on the inverse of the radial distance, which is quadratic rather than linear. This feature is expected, since it has been previously observed for small loops [25], and contributes to validate the developed theory. Numerical simulations demonstrate how in the near-zone of the source ground and lateral waves do not predominate over each other, while the effect of the lateral wave becomes negligible only when the distance of the field point from the loop axis is far greater than the skin depth in the conducting medium.

## 2. PROBLEM FORMULATION

The geometry of the circular loop and the electromagnetic parameters of the plane conducting semi-infinite half-space are illustrated in Fig. 1. For simplicity, only the portion of half-space that lies in close proximity to the circular loop is depicted. The emitter lies at the air-medium interface, has radius $a$, and carries a current equal to $Ie^{j\omega t}$. On the other hand, the dielectric permittivity and electrical conductivity of the medium are indicated with $\epsilon_1$ and $\sigma_1$, respectively, while the magnetic permeability

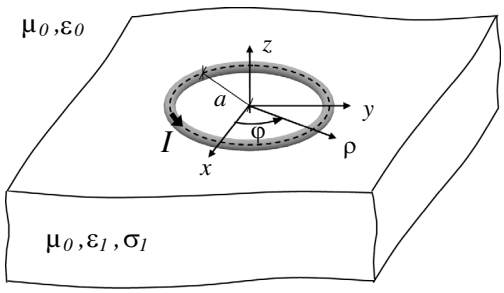


Figure 1: Thin-wire circular loop antenna on the surface of a single-layer conducting medium.

is assumed to be everywhere equal to that of free space $\mu_0$. It is well known [7] that the circular loop can be represented by a uniform magnetic current distribution over the in-loop region of the interface, that is by a distribution of magnetic dipoles lying inside the loop. This allows to express the generated field components in terms of an electric vector potential, resulting from the superposition of the infinitesimal contributions associated with the dipoles. In the air space, it reads [7]

$$\boldsymbol{E} = -\boldsymbol{\nabla} \times \boldsymbol{F}, \tag{1}$$

$$\boldsymbol{H} = -j\omega\epsilon_0 \boldsymbol{F} + \frac{1}{j\omega\mu_0} \boldsymbol{\nabla} \left( \boldsymbol{\nabla} \cdot \boldsymbol{F} \right), \tag{2}$$

where the vector potential $\boldsymbol{F}$ is given by the superposition integral [27, 28]

$$\boldsymbol{F}\left(\boldsymbol{r}\right) = \int_S \bar{\bar{\boldsymbol{G}}}_{\boldsymbol{F}} \left( \boldsymbol{r} | \boldsymbol{\rho'} \right) \cdot d\boldsymbol{m}, \tag{3}$$

being $\boldsymbol{r} = \rho\hat{\boldsymbol{\rho}} + z\hat{\boldsymbol{z}}$ the generic field point, $d\boldsymbol{m}$ the moment of the magnetic dipole at the point $\boldsymbol{\rho'} = \rho'\hat{\boldsymbol{\rho}}'$, located at the $z = 0$ plane, and $\bar{\bar{\boldsymbol{G}}}_{\boldsymbol{F}} \left( \boldsymbol{r} | \boldsymbol{\rho'} \right)$ the three-dimensional dyadic Green's function corresponding to $\boldsymbol{F}$. Finally, $S$ is the circular surface delimited by the edge of the loop. Notice that $\bar{\bar{\boldsymbol{G}}}_{\boldsymbol{F}}$ includes the effects of the material medium, and its physical meaning is as follows. The generic scalar component $G_F^{st}$ is the $s$-component of the vector potential at the field point $\boldsymbol{r}$ produced by a unit-moment $t$-directed magnetic dipole placed at the source point $\boldsymbol{\rho'}$ [28]. For the horizontal loop case, the equivalent magnetic dipoles are directed along the $z$-axis, and, as a consequence, $d\boldsymbol{m} = I dS' \, \hat{\boldsymbol{z}}$. Hence, Eq. (3) simplifies to

$$\boldsymbol{F}\left(\boldsymbol{r}\right) = I \int_S \boldsymbol{G}_F^z \left( \boldsymbol{r} | \boldsymbol{\rho'} \right) dS', \tag{4}$$

where $\boldsymbol{G}_F^z$ is the third column of $\bar{\bar{\boldsymbol{G}}}_{\boldsymbol{F}}$, that is the field due to a unit-moment $z$-directed point source. It should be observed that vertical orientation of dipole sources makes the configuration of the problem symmetrical. This implies that currents in the conducting medium flow only horizontally, and there is no vertical component of the electric field [7]. Thus, the electromagnetic field is transverse electric (TE) with respect to $z$, and, in virtue of Eqs. (1) and (4), the components $F_x$ and $F_y$, as well as $G_F^{xz}$ and $G_F^{yz}$, must be identically zero. Equation (4) turns into

$$\boldsymbol{F}\left(\boldsymbol{r}\right) = I \left[ \int_S G_F^{zz} \left( \boldsymbol{r} | \boldsymbol{\rho'} \right) dS' \right] \hat{\boldsymbol{z}}, \tag{5}$$

where $G_F^{zz}$ is well known and given by [7]

$$G_F^{zz} \left( \boldsymbol{r} | \boldsymbol{\rho'} \right) = \frac{j\omega\mu_0}{2\pi} \int_0^\infty \frac{e^{-u_0 z}}{u_0 + u_1} J_0 \left( \lambda | \boldsymbol{\rho} - \boldsymbol{\rho'} | \right) \lambda \, d\lambda, \tag{6}$$

being $J_n(\cdot)$ the $n$th-order Bessel function, and

$$u_n = \sqrt{\lambda^2 - k_n^2}, \qquad Re[u_n] > 0, \tag{7}$$

$$k_n^2 = -j\omega\mu_0 \left( \sigma_n + j\omega\epsilon_n \right). \tag{8}$$

Interchange of the order of the integrals in Eq. (5), and use of the tabulated result [7]

$$\int_S J_0 \left( \lambda | \boldsymbol{\rho} - \boldsymbol{\rho'} | \right) dS' = \frac{2\pi a}{\lambda} J_0 \left( \lambda\rho \right) J_1 \left( \lambda a \right) \tag{9}$$

allows to express $\boldsymbol{F}$ as

$$\boldsymbol{F} = j\omega\mu_0 I a \left[ \int_0^\infty \frac{e^{-u_0 z}}{u_0 + u_1} J_0(\lambda\rho) \, J_1(\lambda a) d\lambda \right] \hat{\boldsymbol{z}}. \tag{10}$$

It should be observed that Eq. (10) describes the difference between the total field reflected by the material medium and the ideal reflected field, that is the field of an ideal negative image loop [12]. In

fact, when the source lies at the air-medium interface, the image field exactly compensates the direct field generated by the antenna.

The present work is focused on the derivation of the canonical solution for the non-null field components $E_\varphi$, $H_\rho$, and $H_z$ at the air-medium interface ($z = 0^+$). The derivation consists of casting the integral representations for $E_\varphi$ and $H_\rho$ into forms involving only previously evaluated Sommerfeld Integrals. Once the two field components are written in explicit form, an analogous explicit expression for $H_z$ can be deduced by applying Faraday's law.

Use of Eqs. (10) in Eqs. (1) and (2) allows to obtain, after performing the derivatives, the following representations for $E_\varphi$ and $H_\rho$

$$E_\varphi = -j\omega\mu_0 Ia \int_0^\infty \frac{e^{-u_0 z}}{u_0+u_1} J_1(\lambda\rho) J_1(\lambda a)\lambda d\lambda, \tag{11}$$

$$H_\rho = Ia \int_0^\infty \frac{u_0\, e^{-u_0 z}}{u_0+u_1} J_1(\lambda\rho) J_1(\lambda a)\lambda d\lambda, \tag{12}$$

which, after multiplying the numerator and denominator of the fractions under the integral signs by $(u_0 - u_1)$, may be further simplified to

$$E_\varphi = -\frac{j\omega\mu_0 Ia}{k_1^2 - k_0^2}\left(P_0 - P_1\right), \tag{13}$$

$$H_\rho = \frac{Ia}{k_1^2 - k_0^2}\left(Q_0 - Q_1\right), \tag{14}$$

being

$$P_n = \int_0^\infty u_n e^{-u_0 z} J_1(\lambda\rho) J_1(\lambda a)\lambda d\lambda, \tag{15}$$

$$Q_n = \int_0^\infty u_0 u_n e^{-u_0 z} J_1(\lambda\rho) J_1(\lambda a)\lambda d\lambda. \tag{16}$$

Next, use of the identity [29, 11.41.17]

$$J_m(\xi)\, J_m(\psi) = \frac{1}{\pi}\int_0^\pi J_0\left(\eta\right)\cos m\phi\, d\phi, \tag{17}$$

where

$$\eta = \sqrt{\xi^2 + \psi^2 - 2\xi\psi\cos\phi}, \tag{18}$$

makes it possible to rewrite Eqs. (15) and (16) as

$$P_n = \frac{1}{\pi}\int_0^\pi \cos\phi \int_0^\infty u_n e^{-u_0 z} J_0\left(\lambda R\right)\lambda d\lambda\, d\phi, \tag{19}$$

$$Q_n = \frac{1}{\pi}\int_0^\pi \cos\phi \int_0^\infty u_0 u_n e^{-u_0 z} J_0\left(\lambda R\right)\lambda d\lambda\, d\phi, \tag{20}$$

with

$$R = \sqrt{\rho^2 + a^2 - 2a\rho\cos\phi}. \tag{21}$$

To evaluate the $P_n$'s it is convenient to replace $u_n$ in (19) with

$$u_n = \left[\frac{\partial^2}{\partial\zeta^2}\left(\frac{e^{-u_n\zeta}}{u_n}\right)\right]_{\zeta=0}, \tag{22}$$

and, after taking the limit as $z \to 0^+$, make use of the Sommerfeld Identity [30, p. 9, no. 24]

$$\int_0^\infty \frac{e^{-u_n\zeta}}{u_n} J_0\left(\lambda R\right)\lambda d\lambda = \frac{e^{-jk_n\sqrt{R^2+\zeta^2}}}{\sqrt{R^2+\zeta^2}}, \tag{23}$$

so as to obtain

$$P_n = \frac{1}{\pi}\left(\frac{\partial^2 S_n}{\partial \zeta^2}\right)_{\zeta=0}, \tag{24}$$

with

$$S_n = \int_0^{\pi} \frac{e^{-jk_n\sqrt{R^2+\zeta^2}}}{\sqrt{R^2+\zeta^2}} \cos\phi \, d\phi. \tag{25}$$

The explicit form of Eq. (25) is tabulated in [3, (53)–(56)]. It reads

$$S_n = -j\pi k_n \sum_{l=1}^{\infty} \frac{\left(k_n^2 a\rho/2\right)^{2l-1}}{l!\,(l-1)!} \frac{h_{2l-1}^{(2)}(k_n\sqrt{r^2+\zeta^2})}{(k_n\sqrt{r^2+\zeta^2})^{2l-1}}, \tag{26}$$

being $h_l^{(2)}(\cdot)$ the $l$th-order spherical Hankel function of the second kind and $r = \sqrt{\rho^2+a^2}$, and, as a consequence, Eq. (24) turns into

$$P_n = -jk_n \sum_{l=1}^{\infty} \frac{\left(k_n^2 a\rho/2\right)^{2l-1}}{l!\,(l-1)!} \left[\frac{\partial^2}{\partial\zeta^2} \frac{h_{2l-1}^{(2)}(k_n\sqrt{r^2+\zeta^2})}{(k_n\sqrt{r^2+\zeta^2})^{2l-1}}\right]_{\zeta=0} = jk_n^3 \sum_{l=1}^{\infty} \frac{\left(k_n^2 a\rho/2\right)^{2l-1}}{l!\,(l-1)!} \frac{h_{2l}^{(2)}(k_n r)}{(k_n r)^{2l}}. \tag{27}$$

On the other hand, combining Eq. (7) with the Bessel differential equation [31, 32]

$$\left(\frac{\partial^2}{\partial R^2} + \frac{1}{R}\frac{\partial}{\partial R} + \lambda^2\right) C_0(\lambda R) = 0, \tag{28}$$

where $C_0(\cdot)$ is any zeroth-order Bessel function, leads to the equation

$$u_n^2 J_0(\lambda R) = -\left(\frac{\partial^2}{\partial R^2} + \frac{1}{R}\frac{\partial}{\partial R} + k_n^2\right) J_0(\lambda R) = -L_n\left[J_0(\lambda R)\right], \tag{29}$$

which may be used in Eq. (20) to give, in the limit as $z \to 0^+$, the expression

$$Q_n = \frac{1}{\pi}\int_0^{\pi} \cos\phi \, L_0 L_n \left[\int_0^{\infty} \frac{1}{u_0 u_n} J_0(\lambda R)\, \lambda d\lambda\right] d\phi. \tag{30}$$

Evaluation of $Q_0$ is straightforward. In fact, from [30, p. 11, no. 45] it follows that

$$\int_0^{\infty} \frac{1}{u_0^2} J_0(\lambda R)\, \lambda d\lambda = K_0(k_0 R), \tag{31}$$

where $K_0(\cdot)$ is the zeroth-order modified Bessel function of the second kind. This implies that $Q_0$ is null since, in virtue of Eq. (28), $L_0[K_0(k_0 R)] = 0$. Finally, $Q_1$ may be evaluated by proceeding as follows. First, use of the well-known result [30, p. 8, no. 17]

$$\int_0^{\infty} \frac{1}{u_0 u_1} J_0(\lambda R)\, \lambda d\lambda = K_0(\alpha R)\, I_0(\beta R), \tag{32}$$

where $I_0(\cdot)$ is the zeroth-order modified Bessel functions of the first kind, and

$$\alpha = \frac{j(k_1+k_0)}{2}, \qquad \beta = \frac{j(k_1-k_0)}{2}, \tag{33}$$

makes it possible to simplify expression (30), written for $Q_1$, to

$$\begin{aligned} Q_1 &= \frac{1}{\pi}\int_0^{\pi} L_0 L_1\left[K_0(\alpha R)\, I_0(\beta R)\right] \cos\phi \, d\phi \\ &= \frac{2\alpha^2\beta^2}{\pi}\int_0^{\pi} \left[K_2(\alpha R)\, I_2(\beta R) - K_0(\alpha R)\, I_0(\beta R)\right] \cos\phi \, d\phi. \end{aligned} \tag{34}$$

Next, use of the relation [29, 11.41.17]

$$K_m(\xi)\, I_m(\psi) = \frac{1}{\pi}\int_0^{\pi} K_0(\eta)\cos m\phi\, d\phi, \tag{35}$$

permits to rewrite Eq. (34) as

$$Q_1 = \frac{2\alpha^2\beta^2}{\pi^2}\int_0^{\pi}\left(\cos 2\phi' - 1\right)\int_0^{\pi} K_0(\delta R)\cos\phi\, d\phi\, d\phi' = \frac{2\alpha^2\beta^2}{\pi}\int_0^{\pi} K_1(\delta\rho)\, I_1(\delta a)\left(\cos 2\phi' - 1\right) d\phi'$$

$$= -\frac{2\alpha^2\beta^2}{\pi\delta}\frac{\partial}{\partial a}\int_0^{\pi} K_1(\delta\rho)\, I_0(\delta a)\left(\cos 2\phi' - 1\right) d\phi', \tag{36}$$

being

$$\delta = \sqrt{\alpha^2 + \beta^2 - 2\alpha\beta\cos\phi'}. \tag{37}$$

The last integral in Eq. (36) is written in a form suitable for application of addition formulas [29, 11.41.8] and [29, 11.3.7], namely

$$K_1(\delta\rho) = \frac{2\delta}{\alpha\beta\rho}\sum_{m=1}^{\infty} f_m(\rho)\, C_{m-1}^{(1)}\left(\cos\phi'\right), \tag{38}$$

$$I_0(\delta a) = g_0(a) + 2\sum_{l=1}^{\infty}(-1)^l g_l(a)\cos l\phi', \tag{39}$$

with

$$f_m(\rho) = m\, K_m(\alpha\rho)\, I_m(\beta\rho), \tag{40}$$

$$g_l(a) = I_l(\alpha a)\, I_l(\beta a), \tag{41}$$

and where $C_m^{(1)}(\cos\phi')$ denotes the coefficient of $\theta^m$ in the expansion of $\left(1 - 2\theta\cos\phi' + \theta^2\right)^{-1}$ in ascending powers of $\theta$. It yields

$$Q_1 = -\frac{4\alpha\beta}{\pi\rho}\sum_{l=0}^{\infty}(-1)^l\frac{\partial\left[g_l(a)\right]}{\partial a}\sum_{m=1}^{\infty} q_{lm} f_m(\rho), \tag{42}$$

being

$$q_{lm} = \begin{cases} \displaystyle\int_0^{\pi} C_{m-1}^{(1)}\left(\cos\phi'\right)\left(\cos 2\phi' - 1\right)\, d\phi', & l = 0, \\ \displaystyle 2\int_0^{\pi} C_{m-1}^{(1)}\left(\cos\phi'\right)\left(\cos 2\phi' - 1\right)\cos l\phi'\, d\phi', & l > 0, \end{cases} \tag{43}$$

and, since it holds

$$q_{lm} = \begin{cases} \pi, & m = l - 1, \qquad l > 1, \\ -\pi, & m = l + 1, \\ 0, & elsewhere, \end{cases} \tag{44}$$

one obtains

$$Q_1 = \frac{4\alpha\beta}{\rho}\left[f_1\frac{\partial g_0}{\partial a} + \sum_{l=1}^{\infty}(-1)^l\left(f_{l+1} - f_{l-1}\right)\frac{\partial g_l}{\partial a}\right], \tag{45}$$

where the dependences of $f_l$ and $g_l$ on $\rho$ and $a$ have been omitted for better clarity. Finally, applying the recurrence relations for the Bessel functions [31, 9.6.26-9.6.28] provides the explicit form of the $a$-derivatives in Eq. (45), that is

$$\frac{\partial g_0}{\partial a} = \frac{2}{\alpha\beta a}\left[\left(\alpha^2+\beta^2\right) g_1 + 2\alpha\beta g_2\right] + \frac{\partial g_2}{\partial a}, \tag{46}$$

$$\frac{\partial g_l}{\partial a} = \frac{\alpha\beta a}{2\,l}\left(g_{l-1} - g_{l+1}\right), \qquad l > 0. \tag{47}$$

Substitution of Eqs. (27) and (45) in Eqs. (13) and (14), respectively, gives rise to

$$E_\varphi = \frac{\omega\mu_0 Ia}{4\alpha\beta}\left[k_n^3 \sum_{l=1}^{\infty} \frac{\left(k_n^2 a\rho/2\right)^{2l-1}}{l!\,(l-1)!} \frac{h_{2l}^{(2)}\left(k_n r\right)}{\left(k_n r\right)^{2l}}\right]_{n=0}^{n=1}, \tag{48}$$

$$H_\rho = \frac{Ia}{\rho}\left[f_1 \frac{\partial g_0}{\partial a} + \sum_{l=1}^{\infty} (-1)^l \left(f_{l+1} - f_{l-1}\right) \frac{\partial g_l}{\partial a}\right], \tag{49}$$

while from Eq. (48) and Faraday's law, namely

$$\boldsymbol{H} = -\frac{1}{j\omega\mu_0}\boldsymbol{\nabla}\times\boldsymbol{E}, \tag{50}$$

it follows that

$$H_z = -\frac{1}{j\omega\mu_0}\frac{1}{\rho}\frac{\partial\left(\rho E_\varphi\right)}{\partial\rho} = \frac{jIa^2}{4\alpha\beta}\left\{k_n^5 \sum_{l=1}^{\infty} \frac{\left(k_n^2 a\rho/2\right)^{2l-2}}{\left[(l-1)!\right]^2}\left[\frac{h_{2l}^{(2)}\left(k_n r\right)}{\left(k_n r\right)^{2l}} - \frac{\left(k_n\rho\right)^2}{2l}\frac{h_{2l+1}^{(2)}\left(k_n r\right)}{\left(k_n r\right)^{2l+1}}\right]\right\}_{n=0}^{n=1}, \tag{51}$$

where $\{X_n\}_{n=0}^{n=1}$ indicates the difference $X_1 - X_0$. It should be noted that the two contributions in Eqs. (48) and (51), corresponding to $n = 0$ and $n = 1$, are related to the branch-cut integrals arising from deforming the integration path in Eq. (11), so that it is wrapped around the branch lines running from $k_0$ and $k_1$. As such, the two terms describe the above-surface ground wave (associated with $k_0$) and the lateral wave (associated with $k_1$). Analogously, Eq. (49) is the result of the analytical evaluation of the branch-cut integrals originating from Eq. (12), even if one cannot distinguish the contributions of the two waves to the total $H_\rho$-field.

In the far-zone of the antenna, the above-surface ground wave and lateral wave have the characteristics of cylindrical waves travelling in the positive $\rho$-direction. The corresponding analytical expressions may be obtained from Eqs. (48), (49), and (51) by assuming $\rho \gg a$, $r \cong \rho$, and $|k_n|\rho \gg 1$. This allows to replace the spherical Hankel functions in Eqs. (48) and (51) with their asymptotic expansions for large arguments, that is

$$h_l^{(2)}\left(k_n r\right) \cong h_l^{(2)}\left(k_n\rho\right) \cong j^{l+1}\frac{e^{-jk_n\rho}}{k_n\rho}, \tag{52}$$

and to express the $E_\varphi$- and $H_z$-fields as

$$E_\varphi \cong -\frac{j\omega\mu_0 Ia}{4\alpha\beta\rho^2}\left[k_n J_1\left(k_n a\right) e^{-jk_n\rho}\right]_{n=0}^{n=1}, \tag{53}$$

$$\begin{aligned} H_z &\cong -\frac{Ia}{4\alpha\beta\rho^3}\left\{k_n^2\left[j\rho J_1\left(k_n a\right) - a J_0\left(k_n a\right)\right] e^{-jk_n\rho}\right\}_{n=0}^{n=1} \\ &\cong -\frac{jIa}{4\alpha\beta\rho^2}\left[k_n^2 J_1\left(k_n a\right) e^{-jk_n\rho}\right]_{n=0}^{n=1}, \end{aligned} \tag{54}$$

where use has been made of the identity

$$J_m\left(k_n a\right) = \sum_{l=0}^{\infty} \frac{(-1)^l}{l!\,(l+m)!}\left(\frac{k_n a}{2}\right)^{2l+m}. \tag{55}$$

On the other hand, introducing the asymptotic expansions of the modified Bessel functions for large arguments, namely [26, 33, 34]

$$I_l(\beta\rho)\cong\frac{e^{\beta\rho}+(-1)^l je^{-\beta\rho}}{\sqrt{2\pi\beta\rho}}, \tag{56}$$

$$K_l(\alpha\rho)\cong\sqrt{\frac{\pi}{2\alpha\rho}}e^{-\alpha\rho}, \tag{57}$$

makes it possible to rewrite $f_l(\rho)$ in the form

$$f_l(\rho)\cong\frac{l}{2\rho\sqrt{\alpha\beta}}\left[e^{-jk_0\rho}+(-1)^l je^{-jk_1\rho}\right], \tag{58}$$

and express Eq. (49) as

$$H_\rho\cong\frac{Ia}{2\rho^2\sqrt{\alpha\beta}}\left\{e^{-jk_0\rho}\frac{\partial}{\partial a}\left[g_0(a)+2\sum_{l=1}^{\infty}(-1)^l g_l(a)\right]-je^{-jk_1\rho}\frac{\partial}{\partial a}\left[g_0(a)+2\sum_{l=1}^{\infty}g_l(a)\right]\right\}. \tag{59}$$

The quantities in the square brackets of Eq. (59) coincide with the right-hand side of Eq. (39), provided that it is assumed $\phi'=0$ and $\phi'=\pi$, respectively. Thus, use of Eq. (39) in combination with Eq. (33) leads to simplifying Eq. (59) to

$$H_\rho\cong\frac{Ia}{2\rho^2\sqrt{\alpha\beta}}\left[j^n e^{-jk_n\rho}\frac{\partial}{\partial a}I_0(jk_n a)\right]_{n=1}^{n=0}=\frac{Ia}{2\rho^2\sqrt{\alpha\beta}}\left[j^n k_n J_1(k_n a)\,e^{-jk_n\rho}\right]_{n=0}^{n=1}. \tag{60}$$

Expressions (53), (54), and (60) tell us that the far-field results from the interference of two sinusoidal waves, which propagate with the wavenumbers $k_0$ and $k_1$ and decay as $1/\rho^2$ with increasing $\rho$. It should be noted that the presence of the material medium has the effect to change the $\rho$-dependence in the field expressions, from $1/\rho$ to $1/\rho^2$. In fact, the non-null far electric and magnetic field components of the circular loop in free-space are given by the formulas [2]

$$E_\varphi\cong\frac{\omega\mu_0 Ia}{2\rho}J_1(k_0 a)\,e^{-jk_0\rho}, \tag{61}$$

$$H_z\cong\frac{k_0}{\omega\mu_0}E_\varphi, \tag{62}$$

which, except for the $1/\rho$ dependence, are formally similar to each of the two terms in Eqs. (53) and (54). This feature is expected, since it has been previously observed for small loops [26].

## 3. DISCUSSION

To test the correctness and accuracy of the developed theory, expressions (48), (49), and (51) are applied to the computation of the frequency spectra of the $E_\varphi$-, $H_\rho$-, and $H_z$-fields produced on the top surface of a homogeneous clay soil by a circular loop, $100/\pi$ m in radius, which carries 1 A of current. The electrical conductivity and dielectric permittivity of clay are taken to be $\sigma_1 = 25$ mS/m and $\epsilon_1 = 10\,\epsilon_0$ [35–38], respectively, while the field point is located at distance $\rho = 1000/\pi$ m from the loop axis. The field components are computed at 200 frequency points, distributed in the range comprised between 100 Hz and 40 MHz. The obtained results, depicted in Figs. 2–4, are compared with the data provided by numerical integration of Eqs. (1)–(10). Quadpack library included in the Slatec mathematical libraries is used to perform numerical evaluation of the field integrals.

Each solid or dashed curve of Figs. 2–4 is associated with a specific index $l$ at which the sums in Eqs. (48), (49), and (51) are truncated. As is seen, the convergence of the proposed solution is fast, since it suffices to use sums made up of 11 terms (for $E_\varphi$ and $H_z$) and 14 terms (for $H_\rho$) to achieve curves that are in excellent agreement with the exact numerical data. Fast convergence rate is associated with low computation time. For instance, on a single-core 1.8 GHz PC, computation of the spectrum of $|E_\varphi|$ takes only 7 s, which is a negligible time cost if compared to that of Gaussian quadrature, that is about

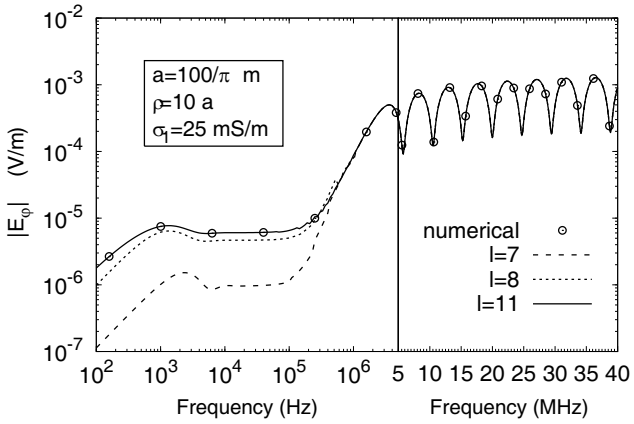


Figure 2: Amplitude-frequency spectrum of $E_\varphi$, computed at distance $\rho = 1000/\pi$ m from the loop axis.

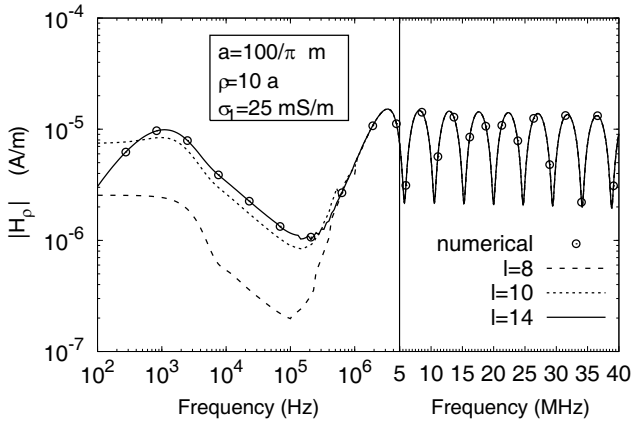


Figure 3: Amplitude-frequency spectrum of $H_\rho$, computed at distance $\rho = 1000/\pi$ m from the loop axis.

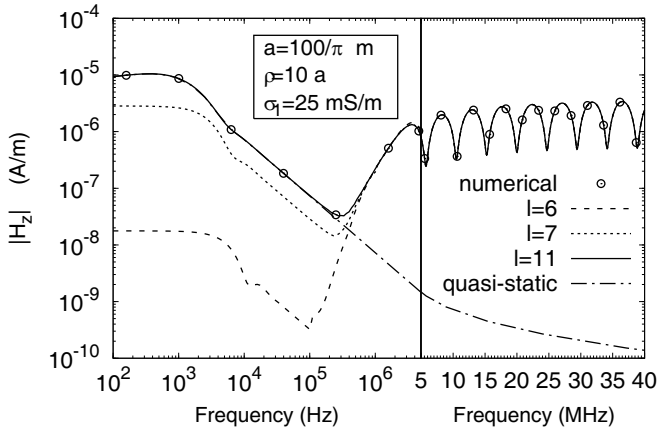


Figure 4: Amplitude-frequency spectrum of $H_z$, computed at distance $\rho = 1000/\pi$ m from the loop axis.

412 s. It should be noted that Fig. 4 also illustrates the behavior of the quasi-static approximation of $H_z$, published in [16]. From a comparison with the outcomes from Eq. (51), truncated at $l = 11$, it emerges that beyond 100 kHz the quasi-static trend and the exact curve start to diverge. In particular, the quasi-static approximation for $H_z$ is valid up to about 210 kHz, where the relative percent error resulting from using it rather than Eq. (51) is equal to 10 % (the generated outcome is $3.4{\cdot}10^{-8}$ A/m instead of $3.8 \cdot 10^{-8}$ A/m).

Figures 2–4 show that the spectra of $|E_\varphi|$, $|H_\rho|$, and $|H_z|$ start to oscillate at frequencies higher than 1 MHz. The oscillatory trend is due to the fact that, at high frequencies, the field point enters the far-zone of the antenna, where, as will be clarified later, the ground wave predominates over the lateral wave. The consequence of this is that, according to Eqs. (53), (54), and (60), the frequency spectra of the field components are dominated by the Bessel function $J_1(k_0 a)$, which, in turn, may be confused with its asymptotic approximation for large arguments, because the antenna has become electrically large ($k_0 a \gg 1$). It reads

$$J_1(k_0 a) \cong \sqrt{\frac{2}{\pi k_0 a}} \sin\left(k_0 a - \frac{\pi}{4}\right), \tag{63}$$

and the amplitudes of $|E_\varphi|$ and $|H_z|$ assume the forms

$$|E_\varphi| \cong \frac{\omega \mu_0 I}{\alpha \beta \rho^2} \sqrt{\frac{k_0 a}{8\pi}} \left|\sin\left(k_0 a - \frac{\pi}{4}\right)\right|, \qquad |H_z| \cong \frac{k_0}{\omega \mu_0} |E_\varphi|. \tag{64}$$

Expressions (64) tell us that the period of the high-frequency oscillatory patterns shown in Figs. 2–4 can be calculated by equating $2k_0a$ to $2\pi$, and then solving for frequency. For $a = 100/\pi$ m the period, which will be referred to as $\tilde{f}$, is equal to

$$\tilde{f} = \frac{1}{2a\sqrt{\mu_0\epsilon_0}} = \frac{3\pi \cdot 10^8}{200} \cong 4.7 \text{ MHz}, \tag{65}$$

a value that is in agreement with the plotted curves.

As anticipated above, at frequencies higher than 1 MHz the effect of the lateral wave is substantially negligible. This aspect is pointed out in Fig. 5, which shows the spectra of the ground- and lateral-wave contributions to the $H_z$-field in a frequency range comprised between 100 Hz and 100 MHz, together with the total field (denoted by points). The electromagnetic parameters of the medium, as well as the

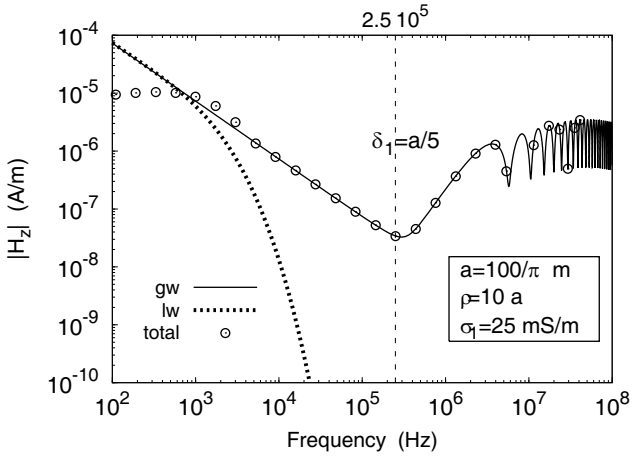


Figure 5: Amplitude-frequency spectra of the total $H_z$-field and its ground-wave (gw) and lateral-wave (lw) components, computed at $\rho = 1000/\pi$ m. The conductivity of the medium is $\sigma_1 = 25$ mS/m.

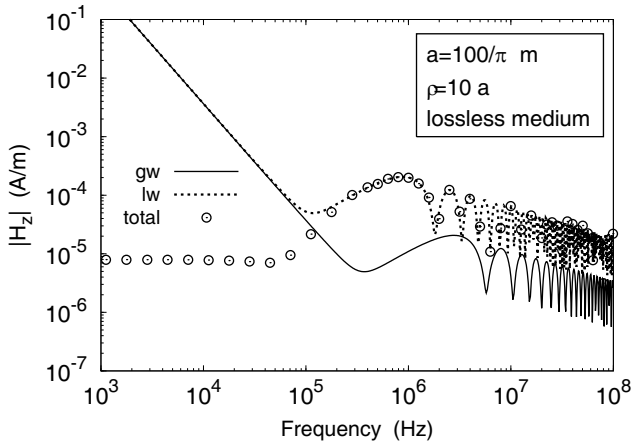


Figure 6: Amplitude-frequency spectra of the total $H_z$-field and its ground-wave (gw) and lateral-wave (lw) components, computed at $\rho = 1000/\pi$ m. The medium is assumed to be lossless.

position of the field point, are taken to be the same as in the previous examples, and computations have been performed truncating the infinite sums in Eq. (51) at $l = 11$. As is seen, at extremely low frequencies the lateral wave interferes destructively with the ground wave, and, as a result, the total field strength is about one order of magnitude smaller than those of the two contributions. When frequency is increased, the lateral-wave field rapidly diminishes in magnitude, and this is strictly related to the reduction of the skin depth $\delta_1$ in the conducting medium. In particular, the lateral wave does not affect the total field if $\delta_1$ is far less than the distance of the field point from the edge of the loop ($|\rho - a|$). This happens, for instance, at the frequency of 250 kHz, when $\delta_1 = a/5$ and $\rho - a = 9a = 45\delta_1$, as shown in Fig. 5.

Following this rationale, increase of $\delta_1$ through a reduction of $\sigma_1$ can mitigate the attenuation of the amplitude-frequency spectrum of the lateral wave. Thus, in the limit as $\delta_1 \to \infty$, corresponding to a lossless medium, the lateral wave is expected to exist even in the far-zone of the antenna. Confirmation of this expectation is provided by Fig. 6, which shows the frequency spectrum of $|H_z|$ obtained under the assumption of lossless dielectric. As is observed, at high frequencies now the lateral wave not only significantly affects the total field, but offers the most important contribution.

To better understand the dependence of the lateral-wave strength on the distance from the edge of the loop, expressed in skin depths, it suffices to take a glance at Fig. 7, which depicts the amplitude of the total $H_z$-field against $\rho$ at 250 kHz (solid line), together with those of the two wave contributions (dashed line and points). The conductivity of the medium has been diminished by two orders of magnitude, from $\sigma_1 = 25$ mS/m down to $\sigma_1 = 0.25$ mS/m. As is seen, at distance $\rho = 1000/\pi = 10\,a$ from the loop

axis the effect of the lateral wave is no longer negligible with respect to that of the ground wave, and this is in agreement with Eq. (54), which provides the following estimate of the ratio between the two contributions

$$\tau = \frac{|H_z^{lw}|}{|H_z^{gw}|} \cong \frac{k_1^2 J_1(k_1 a)}{k_0^2 J_1(k_0 a)} |e^{-jk_1\rho}| \cong 1.1. \tag{66}$$

The proximity of $\tau$ to unity is to be attributed to the fact that $\rho - a$ is only 4.5 times the skin depth $\delta_1$, which is now equal to $2a$. To reduce $\tau$ down to at most 0.1, so as to obtain an ineffective lateral wave, the source-receiver distance $\rho$ must exceed 580 m, which corresponds to $18.2\,a$. Thus, the lateral-wave field may be considered really negligible when $\rho - a > 17.2\,a = 8.6\,\delta_1$, that is, in general, when $\rho - a \gg \delta_1$. For instance, as clearly highlighted by Fig. 7, this occurs when $\rho - a = 20\,a = 10\,\delta_1$.

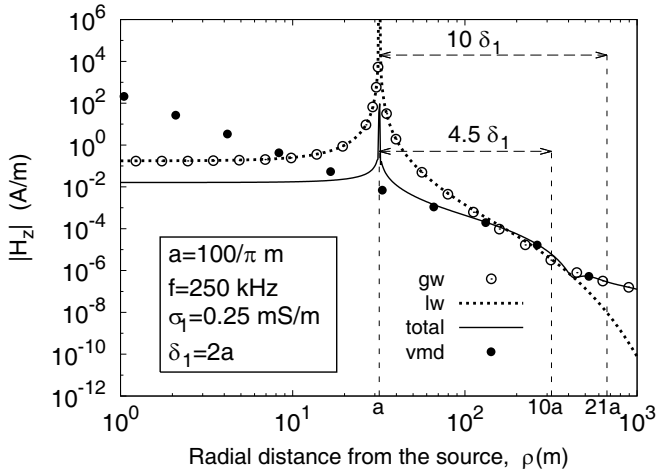


Figure 7: Amplitude of $H_z$ versus source-receiver distance, computed at the frequency of 250 kHz.

Finally, Fig. 7 also depicts the $\rho$-profile of the $H_z$-field arising from the vertical magnetic dipole (i.e., small loop) approximation published in [26]. The fact that, when $\rho$ is significantly greater than $a$, the outcomes from the proposed and small-loop solutions are substantially overlapping, contributes to validate the developed theory.

## 4. CONCLUSIONS

This work has focused on the classical problem of a large circular loop antenna carrying uniform current and situated at the Earth's surface. For such a problem, a totally analytical solution for the surface-to-surface propagation case is currently available, which is valid in the quasi-static frequency range and for the vertical magnetic field component only. In an attempt to overcome the limitations of this approach, the present work has proposed a procedure that allows to derive the exact canonical solution to the problem. The canonical solution describes all the radiated field components, and is valid in both the quasi-static and non-quasi-static frequency regions. Numerical simulations have been performed to illustrate the advantages of using the obtained expressions for the fields. It has been shown how the amplitude-frequency spectrum of the vertical magnetic field arising from the canonical solution is highly accurate, and that, in the considered examples, the quasi-static approximation fails at frequencies higher than 210 kHz. It has been also shown that computational cost of the canonical solution is negligible with respect to that of numerical techniques commonly used to evaluate Sommerfeld-type integrals. Finally, the field components are given in a form that makes it possible to separately study the above surface ground- and lateral-wave contributions in a wide frequency range.

## REFERENCES


1. Foster, D., "Loop antennas with uniform current," *Proceedings of the IRE*, Vol. 32, 603–607, 1944.
2. Balanis, C. A., *Antenna Theory: Analysis and Design*, 2nd Edition, John Wiley & Sons, New York, 1997.
3. Werner, D. H., "An exact integration procedure for vector potentials of thin circular loop antennas," *IEEE Transactions on Antennas and Propagation*, Vol. 44, 157–165, 1996.
4. Singh, N. P. and T. Mogi, "Electromagnetic response of a large circular loop source on a layered earth: A new computation method," *Pure and Applied Geophysics*, Vol. 162, 181–200, 2005.
5. Wait, J. R., "Fields of a horizontal loop antenna over a layered half-space," *Journal of Electromagnetic Waves and Applications*, Vol. 9, 1301–1311, 1995.
6. Palacky, G. J., "Resistivity characteristics of geologic targets," *Electromagnetic Methods in Applied Geophysics*, edited by M. N. Nabighian, Vol. 1, 52–129, SEG, Tulsa, Oklahoma, 1988.
7. Ward, S. H. and G. W. Hohmann, "Electromagnetic theory for geophysical applications," *Electromagnetic Methods in Applied Geophysics, Theory – Volume 1*, M. N. Nabighian (ed.), 131–308, SEG, Tulsa, Oklahoma, 1988.
8. Parise, M., "Efficient computation of the surface fields of a horizontal magnetic dipole located at the air-ground interface," *International Journal of Numerical Modelling: Electronic Networks, Devices and Fields*, Vol. 29, 653–664, 2016.
9. Overfelt, P., "Near fields of the constant current thin circular loop antenna of arbitrary radius," *IEEE Transactions on Antennas and Propagation*, Vol. 44, 166–171, 1996.
10. Parise, M., "An exact series representation for the EM field from a circular loop antenna on a lossy half-space," *IEEE Antennas and Wireless Prop. Letters*, Vol. 13, 23–26, 2014.
11. Zhdanov, M. S., *Geophysical Electromagnetic Theory and Methods*, Elsevier, Amsterdam, 2009.
12. Parise, M., "Full-wave analytical explicit expressions for the surface fields of an electrically large horizontal circular loop antenna placed on a layered ground," *IET Microwaves, Antennas & Propagation*, Vol. 11, 929–934, 2017.
13. Parise, M., "On the use of cloverleaf coils to induce therapeutic heating in Tissues," *Journal of Electromagnetic Waves and Applications*, Vol. 25, 1667–1677, 2011.
14. Boerner, D. E., "Controlled source electromagnetic deep sounding: Theory, results and correlation with natural source results," *Surveys in Geophysics*, Vol. 13, No. 4–5, 435–488, 1992.
15. Shastri, N. L. and H. P. Patra, "Multifrequency sounding results of laboratory simulated homogeneous and two-Layer earth models," *IEEE Trans. Geosci. Remote Sensing*, Vol. 26, No. 6, 749–752, 1988.
16. Parise, M., "Quasi-static vertical magnetic field of a large horizontal circular loop located at the earth's surface," *Progress In Electromagnetics Research Letters*, Vol. 62, 29–34, 2016.
17. Kong, J. A., L. Tsang, and G. Simmons, "Geophysical subsurface probing with radio-frequency interferometry," *IEEE Transactions on Antennas and Propagation*, Vol. 22, No. 4, 616–620, 1974.
18. Singh, N. P. and T. Mogi, "Inversion of large loop transient electromagnetic data over layered earth models," *Jour. Fac. Sci Hokkaido Univ. Ser. VII*, Vol. 12, No. 1, 41–54, 2003.
19. Farquharson, C. G., D. W. Oldenburg, and P. S. Routh, "Simultaneous 1D inversion of loop–loop electromagnetic data for magnetic susceptibility and electrical conductivity," *Geophysics*, Vol. 68, No. 6, 1857–1869, 2003.
20. Guptasarma, D. and B. Singh, "New digital linear filters for Hankel $J_0$ and $J_1$ transforms," *Geophysical Prospecting*, Vol. 45, No. 5, 745–762, 1997.
21. Singh, N. P. and T. Mogi, "Effective skin depth of EM fields due to large circular loop and electric dipole sources," *Earth Planets Space*, Vol. 55, 301–313, 2003.
22. Kong, F. N., "Hankel transform filters for dipole antenna radiation in a conductive medium," *Geophysical Prospecting*, Vol. 55, No. 1, 83–89, 2007.
23. Parise, M., "A study on energetic efficiency of coil antennas used for RF diathermy," *IEEE Antennas and Wireless Prop. Letters*, Vol. 10, 385–388, 2011.

24. Alford, A. and A. Kandoian, "Ultrahigh-frequency loop antennas," *Electrical Engineering*, Vol. 59, 843–848, 1940.
25. Parise, M., "On the surface fields of a small circular loop antenna placed on plane stratified earth," *International Journal of Antennas and Propagation*, Vol. 2015, 1–8, 2015.
26. Parise, M., "Exact electromagnetic field excited by a vertical magnetic dipole on the surface of a lossy half-space," *Progress in Electromagnetics Research B*, Vol. 23, 69–82, 2010.
27. Tai, C., *Dyadic Green functions in electromagnetic theory*, IEEE Press, New York, 1994.
28. Mosig, J. R., R. C. Hall, and F. E. Gardiol, "Numerical analysis of microstrip patch antennas," *Handbook of Microstrip Antennas*, J. R. James and P. S. Hall (eds.), Peter Peregrinus Ltd., London, UK, 1989.
29. Watson, G. N., *A Treatise on the Theory of Bessel Functions*, Cambridge University Press, Cambridge, UK, 1994.
30. Erdelyi, A., *Tables of Integral Transforms — Vol. 2*, McGraw-Hill, New York, 1954.
31. Abramowitz, M. and I. A. Stegun, *Handbook of Mathematical Functions with Formulas, Graphs, and Mathematical Tables*, Dover, New York, 1964.
32. Parise, M., "Exact EM field excited by a short horizontal wire antenna lying on a conducting soil," *AEU-International Journal of Electronics and Communications*, Vol. 70, 676–680, 2016.
33. Parise, M., "Second-order formulation for the quasi-static field from a vertical electric dipole on a lossy half-space," *Progress In Electromagnetics Research*, Vol. 136, 509–521, 2013.
34. Gradshteyn, I. S. and I. M. Ryzhik, *Table of Integrals, Series, and Products*, Academic Press, New York, 2007.
35. Davis, J. L. and A. P. Annan, "Ground-penetrating radar for high-resolution mapping of soil and rock stratigraphy," *Geophysical Prospecting*, Vol. 37, 531–551, 1989.
36. Daniels, D. J., *Ground Penetrating Radar*, Institution of Engineering and Technology, London, UK, 2004.
37. Parise, M., "An exact series representation for the EM field from a vertical electric dipole on an imperfectly conducting half-space," *Journal of Electromagnetic Waves and Applications*, Vol. 28, No. 8, 932–942, 2014.
38. Telford, W. M., L. P. Geldart, and L. E. Sheriff, *Applied Geophysics*, Cambridge University Press, Cambridge, UK, 1990.